Solar-Terrestrial Physics. 2024. Vol. 10. Iss. 2. P. 13–25. DOI: 10.12737/stp-102202402. © 2024
L.S. Rakhmanova, A.A. Khokhlachev, M.O. Riazantseva, Y.I. Yermolaev, G.N. Zastenker. Published by INFRA-M Academic Publishing House

UDC 523.62-726
DOI: 10.12737/stp-102202402

Received December 04, 2023
Accepted February 21, 2024

TURBULENCE DEVELOPMENT BEHIND THE BOW SHOCK DURING DISTURBED AND UNDISTURBED SOLAR WIND

L.S. Rakhmanova
Space Research Institute RAS,
Moscow, Russia, rakhlud@gmail.com

A.A. Khokhlachev
Space Research Institute RAS,
Moscow, Russia, aleks.xaa@yandex.ru

M.O. Riazantseva
Space Research Institute RAS,
Moscow, Russia, orearm@gmail.com

Yu.I. Yermolaev
Space Research Institute RAS,
Moscow, Russia, yermol@cosmos.ru

G.N. Zastenker
Space Research Institute RAS,
Moscow, Russia, gzastenk@iki.rssi.ru

Abstract. Magnetosheath is a transition layer between the solar wind and the magnetosphere and may contribute to the geoeffectiveness of various large-scale interplanetary phenomena. In this paper, we examine the dynamics of the turbulent fluctuation spectra behind the bow shock during undisturbed solar wind and when interplanetary coronal mass ejections and corotation interaction regions interact with the magnetosphere. The study is based on statistical analysis of the turbulence features inside the magnetosheath at different distances from the bow shock. We demonstrate that the turbulence features change when plasma crosses the bow shock for the solar wind of all types and they usually recover when plasma moves away from the bow shock. However, peculiarities in the turbulence development occur during interplanetary coronal mass ejections. Moreover, during disturbed solar wind there are relations between the turbulence features at the sub-ion scales and background plasma parameters such as plasma parameter β, the angle θ_{BN} between the interplanetary magnetic field and the local bow shock normal, solar wind bulk velocity, and the distance to the magnetosheath boundaries.

Keywords: solar wind, magnetosheath, turbulence, space plasma.

INTRODUCTION

Geoeffectiveness of large-scale phenomena such as interplanetary coronal mass ejections (ICMEs), compression regions in front of them (sheaths), as well as coroting interaction regions (CIRs) has been repeatedly demonstrated by experimental statistical studies [Yermolaev et al., 2015]. A number of studies have pointed out the special role of sheaths and CIRs in the response of the magnetosphere and ionosphere [Yermolaev et al., 2015; Barkhatov et al., 2019, 2001]. Solar wind (SW) plasma and the interplanetary magnetic field (IMF) do not, however, directly affect the magnetosphere — they first pass through the bow (near-Earth) shock wave (BS) and the transition region behind it, the magnetosheath (MSH). Experimental data shows that a high level of variations in all MSH parameters whose source is enhanced wave activity [Schwartz, 1996; Lacombe, Belmont, 1995] and the occurrence of small-scale processes can lead to a significant modification of SW plasma and magnetic structures [Rakhmanova et al., 2016]. This MSH effect may be important for the analysis of solar-terrestrial relations despite the fact that experimental studies of features of the development of turbulent fluctuations in MSH under various SW phenomena have been carried out quite rarely (see the review [Rakhmanova et al., 2023]).

The totality of plasma processes occurring in a wide range of scales can be considered as a cascade of turbulent fluctuations, i.e. fluctuation power distribution over scales. Analysis of the turbulent fluctuation spectrum makes it possible to study features of the development of the turbulent cascade, including plasma processes on different scales, and compare them under different conditions. In SW plasma and MSH, the turbulent fluctuation spectrum is generally power-law between the characteristic plasma scales on which the spectrum breaks, and each spectral region features a specific power exponent. The type of the processes occurring in each of the scale ranges is described and physically justified in [Schekochihin et al., 2009; Kiyani et al., 2015]. It is now believed that on scales over ~10^6 km, which are comparable to the interplanetary phenomena such as ICMEs or processes on the Sun, energy is pumped into the system and, according to experimental data, the spectrum has a –1 power exponent (slope). At scales smaller than the gyroradius and/or the proton inertial length (also known as kinetic scales), the system's energy begins to be transferred to particles and turns into heat, and the spectrum exhibits a slope from –2.9 to –2.33 according to various theoretical predictions and experimental descriptions. In space plasma, these scale ranges (energy pumping and its dissipation) differ by several orders of magnitude and the so-called inertial cascade region is formed between them, where the sys-

tem's energy is transferred from larger to small scales according to the universal law independent of the energy source and methods of its dissipation. This scale range, also known as magnetohydrodynamic (MHD) scales, features spectra with an exponent of –5/3 (the so-called Kolmogorov spectrum). Spectra with such exponents are often observed under quiet conditions in plasma for fluctuations in the magnetic field [Borovsky, 2012], as well as for fluctuations in the ion flux\plasma density [Chen et al., 2013; Riazantseva et al., 2015]. In the approximation of isotropy of fluctuations, turbulence spectra in magnetized plasma are described in [Iroshnikov, 1963; Kraichnan, 1965] in which the spectrum on MHD scales $k^{-3/2}$. This has been confirmed by experimental data [Borovsky, 2012]. Yet, the assumption of plasma isotropy does not find empirical support in most situations in SW. Taking anisotropy into account [Goldreich, Spridar, 1995] made it possible to describe scaling, most often observed in experiments; however, in this work plasma is assumed to be incompressible, which does not fully correspond to measurements either.

In recent years, some experimental studies have shown that the cascade of fluctuations can extend to electron scales. It is supposed that between ion and electron scales a small-scale (electron) inertial region of cascade is formed and dissipation occurs on electron scales (see [Alexandrova et al., 2009; Huang et al., 2014] and discussion in [Alexandrova et al., 2013]). To date, the cascade of fluctuations on electron scales has been investigated relatively rarely due to the lack of available experimental data on near-Earth plasma with an adequate sampling rate and low noise. Turbulence in SW has been studied extensively for several decades (see reviews [Bruno, Carbone, 2013; Alexandrova et al., 2013]).

Peculiarities of the development of turbulence behind BS have been observed for a long time, in particular in experiments on radio translucence of the disturbed subsolar MSH region [Barkhatov et al., 2001]. Full-scale satellite studies became possible later with the advent of a sufficient number of spacecraft in this region. The formation of a cascade of turbulent fluctuations in MSH is significantly affected by the boundaries (magnetopause and BS) that can destroy relations in the cascade [Huang et al., 2017; Sahraoui et al., 2020] or set a preferential direction for the development of the cascade [Sahraoui et al., 2006]. Moreover, it has been repeatedly noted that MSH plasma features a compression component of variations as opposed to the Alfvén (mostly) turbulence in undisturbed SW [Huang et al., 2017]. Local, albeit multipoint, studies of turbulent plasma have been more often performed in the MSH, using data from spacecraft such as Cluster [Sahraoui et al., 2006; Alexandrova et al., 2006, 2008; Yordanova et al., 2008] and MMS [Bandyopadhyay et al., 2020; Chen, Boldyrev, 2017; Macek et al., 2018; Roberts et al., 2019; Yordanova et al., 2020]. The distribution of spectral characteristics of turbulent fluctuations in MSH has begun to be studied fairly recently [Huang et al., 2017; Rakhmanova et al., 2018a; Rakhmanova et al., 2018b; Li et al., 2020]. Statistical analysis indicates that the turbulent cascade evolves when plasma enters MSH and propagates to flanks and magnetopause. For example, in dayside MSH there is no Kolmogorov scaling on MHD scales for magnetic field fluctuations (incompressible component), whereas when plasma approaches flanks, spectra with the Kolmogorov slope of –5/3 are recorded [Huang et al., 2017]. On MSH flanks for ion flux fluctuations (i.e., for the compressible component), it is shown that the Kolmogorov scaling on MHD scales is generally characteristic of regions near the magnetopause, and deviations from it are observed near BS [Rakhmanova et al., 2018b]. On kinetic scales, statistical studies demonstrate a flattening of the magnetic field fluctuation spectra during propagation from BS to the magnetopause [Huang et al., 2017; Li et al., 2020] and from the subsolar region to flanks [Huang et al., 2017]. For ion flux fluctuations, the spectrum slope on kinetic scales was also shown to change on average from –3.2 to –2.8 when moving away from BS and approaching the magnetopause. Statistical analysis has not revealed unambiguous links between turbulence characteristics in MSH and plasma and magnetic field parameters in SW [Li et al., 2020; Rakhmanova et al., 2020a].

In-depth analysis of individual events has revealed that not in all cases there is a deviation from the Kolmogorov scaling behind BS [Rakhmanova et al., 2019]. Preliminary statistical analysis carried out in the above work has shown that the Kolmogorov scaling directly behind BS is most often observed for periods of quiet SW, whereas the most significant deviation of the spectra from the Kolmogorov type on MHD scales occurs during the appearance of sheaths before ICMEs. Further comparison of different experimental data presented in the literature [Rakhmanova et al., 2021] has indicated that the presence or absence of Kolmogorov scaling is most likely determined by BS properties (significant differences in the development of turbulence behind quasi-parallel and quasi-perpendicular BS) and by large-scale properties of incoming SW. Note that in SW for ICMEs and sheaths in front of them there is a difference in characteristics between fluctuation spectra on kinetic scales: on average, for disturbed SW streams the spectra are steeper (with average slopes of –3.15 for sheaths and –3.0 for ICMEs) than for undisturbed SW (with an average slope of –2.8) [Riazantseva et al., 2020], which may also lead to differences between turbulence characteristics in MSH.

Study of the evolution of turbulent fluctuation spectra in MSH based on multipoint measurements has revealed that the development of turbulence behind BS is different under quiet and disturbed SW conditions [Rakhmanova et al., 2020b, 2022]. In particular, it was shown that for disturbed SW, characterized by a high degree of plasma compression such as sheaths in front of ICMEs or in front of high-speed streams from coronal holes (CIR), plasma propagation to flanks is accompanied by increased compression fluctuations on kinetic scales, whereas this is not observed for quiet SW and ICMEs.

Nonetheless, the multipoint analysis based on experimental data does not provide sufficiently extensive and evenly distributed statistics in space due to the difficulty in selecting data from various spacecraft and specifics

of their orbits. In this paper, to verify the effect of SW type on the dynamics of turbulent fluctuation spectrum behind BS, we perform a statistical analysis of measurements from one satellite in MSH, taking into account the type of incoming SW and position relative to boundaries. The analysis is based on data from the Themis mission satellites for 2008 and 2014. We compare turbulence characteristics in dayside MSH and on flanks for SW of various types and examine the difference between dependences of these characteristics on some plasma and magnetic field parameters in both SW and MSH, as well as on the position of the satellite relative to MSH boundaries.

1. DATA AND ANALYSIS METHOD

We have used measurements from five Themis satellites [Angelopoulos, 2008] for 2008 and 2014. These periods coincided with solar minimum and maximum respectively, and were chosen to ensure the maximum variety of conditions in incoming SW. Moreover, in 2008 the Themis satellites were generally in dayside MSH or on the near flank (X_{GSE}>–10 R_E), whereas in 2014 two of the five satellites were in the Moon's orbit and crossed MSH on the far flanks (X_{GSE}~–50 R_E), which also provided coverage of various MSH regions. To assess SW conditions, we employed plasma measurements with the SWE (Solar Wind Experiment) instrument [Ogilvie et al., 1995] and measurements with the MFI (Magnetic Field Investigation) magnetometer [Lepping et al., 1995] on the WIND satellite at the Lagrange point L1.

The Themis satellites' orbits in 2008 were arranged so that all five satellites crossed MSH in different regions with X_{GSE}>–10R_E during the year. In 2014, two satellites (Themis-B and Themis-C) crossed MSH in the tail (X_{GSE}~–50R_E), whereas the remaining satellites entered MSH in its dayside. The satellites' orbits during different time periods are described in detail on the mission's website [https://themis.ssl.berkeley.edu/orbits]. In this paper, we focus on the distribution of turbulence characteristics in different MSH regions; therefore, for periods when the satellites simultaneously crossed MSH at small (~1R_E) distances from each other we take data from only one satellite. This approach allows us to avoid an artificial increase in statistics.

For the analysis, we have selected all data intervals when the satellite was in MSH for at least 1.5 hrs and at the same time magnetic field measurements with FGM (Fluxgate Magnetometer) [Auster et al., 2008] at 0.25 s temporal resolution were available. For each of the intervals, we estimated the plasma propagation time between the WIND satellite at the Lagrange point L1 and the corresponding Themis satellite. To do this, at the first stage the shift T_0 was determined as the ratio of the distance between the satellites along the Sun—Earth line and the SW speed average over the interval. At the second stage, we calculated the correlation coefficient between the plasma density measured on both satellites and reduced to a time grid with the same temporal resolution for time shifts ranging from –40 to +40 min relative to the shift T_0. The shift corresponding to the maximum correlation coefficient was taken for further analysis. At the third stage, we manually analyzed all the intervals in view of the shift, and in the cases when the cross-correlation analysis did not give adequate results we corrected the shift according to the visual coincidence of plasma structures recorded by the two satellites during the period of interest. The obtained intervals lasted from 1.5 to 11 hrs, ~600 hrs in total.

Each of the obtained intervals was divided into subintervals with 68 min duration, which is a compromise between quasi-stationarity of the flux in a subinterval and the number of measurement points required for further spectral analysis. In this case, the step between two subsequent subintervals was taken equal to half the subinterval length, i.e. 34 min, so that when dividing a long interval into subintervals we could take into account the information related to the subintervals' boundaries. We have obtained 1087 subintervals and for each of them have determined plasma and magnetic field parameters at the measurement point in MSH, as well as SW plasma and magnetic field parameters derived from satellite data at L1 with allowance for plasma propagation time.

For each subinterval, we found the angle θ_{BN} between IMF and the normal to BS at the point of plasma entry into MSH. The method for finding the angle is based on tracing the measurement point in MSH to BS along the flow line, determined by the Spreiter model [Spreiter et al., 1966], and on using WIND data as an SW monitor; the method is detailed in [Shevyrev et al., 2003]. The angle θ_{BN} is known as an important parameter controlling the level of fluctuations and small-scale dynamics in MSH [Greenstadt, 1972; Shevyrev et al., 2003]. In this paper, in order to avoid the influence of this parameter on the results, we deal only with the events corresponding to MSH behind quasi-perpendicular BS (θ_{BN}>45°), 866 in total.

For each subinterval, we determined the distance from the measurement point in MSH to the boundaries (magnetopause and shock wave), which is characterized by D from 0 (corresponds to the magnetopause) to 1 (corresponds to BS). The given distance is defined by predicting the position of the magnetopause [Shue et al., 1998] and BS [Verigin et al., 2001] depending on SW parameters for each subinterval.

For all the subintervals considered, we have determined SW types from the catalog compiled by Yermolaev et al. [2009] [http://www.iki.rssi.ru/pub/omni]. The following SW types have been identified: slow (33 % of cases), fast (16 %), heliospheric current sheet (8 %), ejecta-type ICMEs (14 %), magnetic clouds (MC, 3 %), sheaths in front of them (1 %), and corotating interaction regions (13 %). In 12 % of cases, the beginning and end of the event corresponded to different SW types and it was impossible to uniquely identify the SW type for the subinterval. Since slow, fast SW, and the heliospheric current sheet belong to quiet quasi-stationary SW streams and no difference between characteristics of the turbulent fluctuation spectra for these types has been previously observed [Riazantseva et al., 2020], in this work we classify them into the common type of undisturbed SW. Figure 1 indicates the location of observa-

tion points in MSH. The magnetopause and BS are shown schematically; the location of the points outside the depicted region does not mean that the satellite is located outside MSH for a particular event, but it is related to the dynamics of MSH boundaries when SW parameters change. Color depicts events related to the selected SW types. Vertical dashed lines denote the division of statistics into dayside MSH and flank, discussed below. It can be seen that despite the extensive statistics the number of sheath-type subintervals is small and such events were observed only on the MSH flank. For this reason, we omitted the sheath events from statistical analysis. Magnetic clouds were examined together with ejecta events in the general group related to ICMEs.

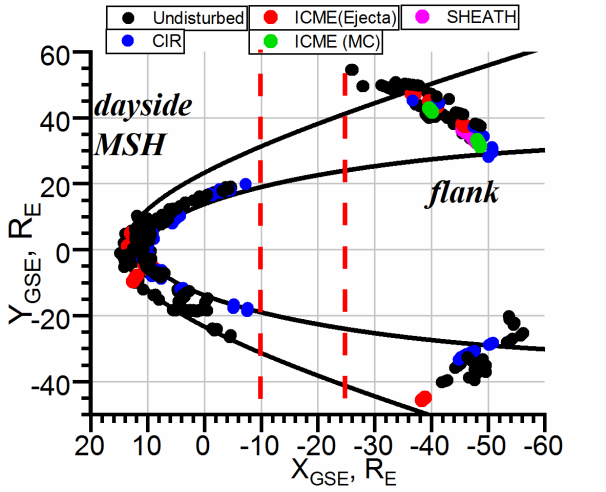

Figure 1. Location of satellites for the events of interest. Color denotes solar wind types; vertical dashed lines indicate the division of statistics into dayside MSH and flank

Note that when studying the turbulent cascade on the basis of experimental data, it is impossible to obtain energy distribution on spatial scales at each instant of time since satellite measurements are carried out in time. In this case, the Taylor hypothesis is generally applied [Taylor, 1938]. According to this hypothesis, it is possible to unambiguously linearly link time and spatial scales if the plasma velocity significantly exceeds the wave mode propagation velocity in plasma, which is almost always the case in SW and often outside the MSH subsolar region. Based on theoretical descriptions and simulation, Klein et al. [2014] have shown that when the ratio of the plasma bulk speed to the Alfvén speed exceeds 0.3, the use of the Taylor hypothesis does not lead to changes in the spectrum shape during transition from spatial to temporal scales. In this paper, we exclude the events (~4 %) that do not meet this criterion from consideration.

Besides the limitations on plasma velocity, the Taylor hypothesis is inapplicable to whistler turbulence since whistlers have a high velocity comparable to the flow velocity. Studies show, however, that whistlers are relatively rare in MSH plasma and on scales smaller than those considered in this paper [Vörös et al., 2019; Lacombe et al., 2014]. It is, therefore, further assumed that the Taylor hypothesis is applicable to all the selected events.

Fourier analysis of fluctuations in the magnetic field magnitude was carried out for each of the subintervals (events) considered. Spectra were obtained using the discrete Fourier transform. The frequency range of interest was then divided into 100 parts on a logarithmic frequency scale, for each we calculated the average power spectral density and smoothed it with a running average by nine points. This procedure provided a spectrum suitable for approximation, while preserving its characteristic features. Next, an automated procedure was made for selecting linear parts of the spectrum and approximating them with power functions, which was then verified manually. All spectra with ambiguous approximation (~15 %) were eliminated from consideration.

Figure 2, *a–c* displays density, velocity modulus and components, as well as magnetic field magnitude and components in MSH for August 28, 2008 from Themis-D measurements. The subinterval used for the frequency spectrum analysis is highlighted in gray. Panel *d* shows the magnetic field magnitude fluctuation spectrum for the given subinterval and its approximation. In this event, two frequency ranges are well traced in the spectrum, in which the spectrum can be approximated by power

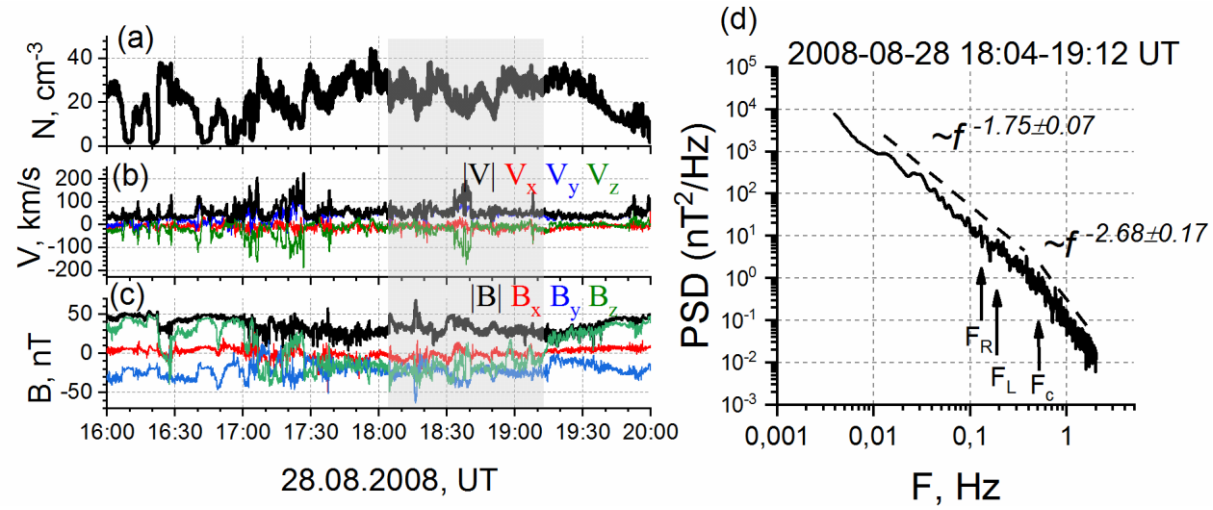

Figure 2. August 28, 2008 event: plasma density (*a*); plasma velocity modulus and components in MSH (*b*); magnetic field magnitude and components (*c*); spectrum of magnetic field magnitude fluctuations (*d*) for the interval highlighted on panels *a–c*

functions with exponents (slopes) P_1=–1.75±0.07 and P_2=–2.68±0.17. The spectrum slope on MHD scales is close to the Kolmogorov one (–5/3), which is usually observed in MSH when plasma moves away from BS and from the subsolar region. After the break, on kinetic scales the spectrum slope is close to –8/3, which is in agreement with some theoretical descriptions [Boldyrev, Perez, 2012]. Figure 2 exhibits characteristic plasma frequencies on ion scales: proton gyrofrequency F_c; the frequency $F_R=V/(2\pi R)$ defined by the Larmor radius $R=V_T/\omega_s$, where V_T is the thermal velocity of particles, $\omega_c=2\pi F_c$; the frequency due to the proton inertial length $F_L=V/(2\pi L)$, where $L=c/\omega_p$, ω_p is the proton plasma frequency. The spectrum break is seen to occur at frequencies close to the characteristic plasma frequencies, as has been repeatedly shown in experimental studies [Chen et al., 2014; Safránková et al., 2015]. Yet, in this work we do not calculate the exact spectrum break frequency since it is impossible to reliably determine it for most cases owing to the presence of some features (peaks, plateaus) in the spectra in dayside MSH.

Figure 3, as in Figure 2, gives an example of Themis-C measurements made on October 14, 2008. In this case, the spectrum features a wide peak at frequencies corresponding to the transition from MHD to kinetic scales.

The automated approximation procedure enabled us to find the frequency at which a peak appears in the spectrum and to make an approximation for the frequency range below the peak, eliminating its effect on the measured spectrum slope. At the same time, a decrease in the number of points causes approximation errors to increase. The approximation is not performed if the number of points in the resulting range is less than 25. The presence of a peak in spectra leads to the fact that reliable approximation on MHD scales cannot be made for all events: in ~50 % of cases, the approximation is impossible. For these cases, the approximation is carried out only on kinetic scales. In this example, the spectrum slope on MHD and kinetic scales P_1=–1.1±0.1 and P_2=–2.9±0.2 respectively, which is often observed in dayside MSH [Huang et al., 2017].

2. RESULTS

2.1. Statistical analysis

In order to examine the difference between turbulence characteristics in dayside MSH and on flanks, it is necessary to determine which region in MSH can be attributed to the flanks as applied to the statistics obtained. Figure 4 shows slopes of spectra as function of X_{GSE}. Each point corresponds to interval average X_{GSE} with a width of 10 R_E; errors in determining the average in these intervals are indicated as errors; the numbers next to the points indicate the number of events for each interval. It is clearly seen that there are two X_{GSE} ranges within which the slopes vary insignificantly: (15÷–10)R_E and (–25÷-55)R_E. Thus, turbulence characteristics change, on average, in the coordinate range X_{GSE}=(–10÷–25)R_E, and two sample subsets with coordinate ranges (15÷–10)R_E and (–25÷–55)R_E can be considered separately as dayside MSH and flank regions (see below).

Figure 5, *a* illustrates the distribution of spectrum slopes on MHD scales for a subsolar region (red) and for flanks (green) for all the events without separation by SW type. It is clearly seen that in the subsolar region the spectrum slopes differ significantly from Kolmogorov ones and are close to –1 on MHD scales. At the same time, on kinetic scales a slope averages –2.9. This result is consistent with the results of statistical analysis for magnetic field fluctuation spectra [Huang et al., 2017].

On MSH flanks, properties of the fluctuation spectra change significantly. Slopes on MHD scales have an average value of –1.5, which is closer to –5/3 typical of the Kolmogorov scaling, but does not fully correspond to it. Note that a number of theoretical descriptions of turbulence [Iroshnikov, 1963; Kraichnan, 1965] suggest that a spectrum slope is –3/2 on MHD scales. Nonetheless, due to the fact that these theories have not been confirmed during decades of experimental research in SW (see discussion [Schekochihin et al., 2009]), there is no reason to assume their applicability to MSH flanks. On kinetic scales, the spectra become significantly flatter, with an average slope of –2.1, which is close to –7/3 predicted by a number of turbulence development theories [Schekochihin et al., 2009].

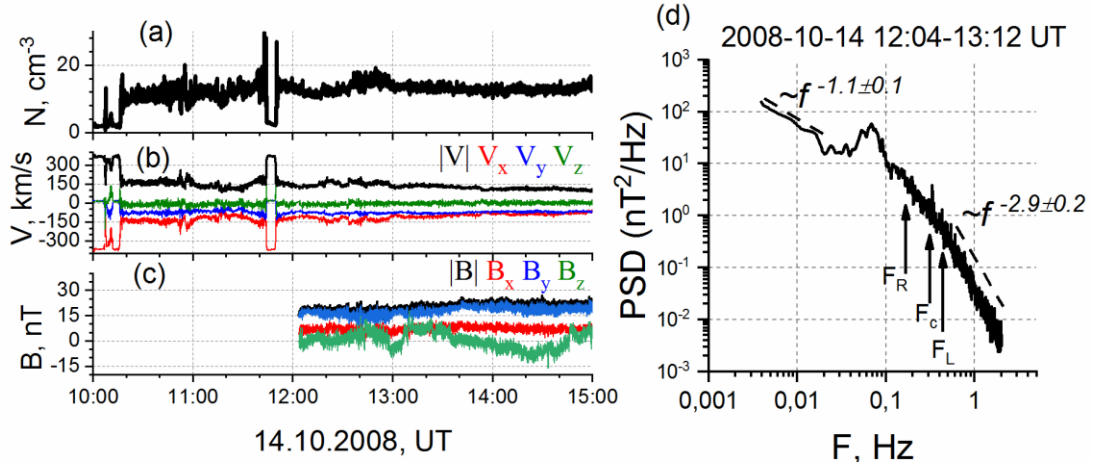

Figure 3. October 14, 2008 event: designations are the same as in Figure 2

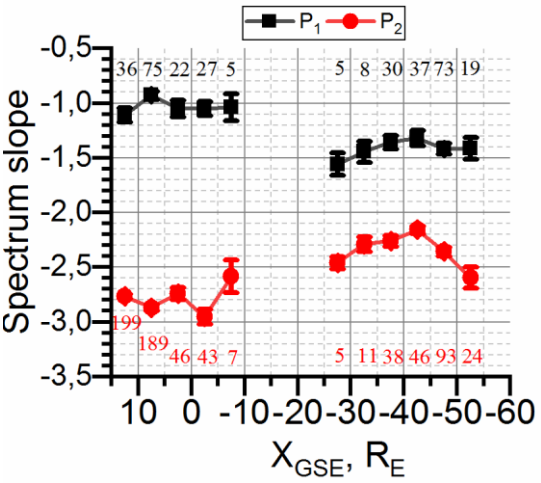

Figure 4. Averaged spectrum slopes as function of X_{GSE} on MHD (black) and kinetic (red) scales

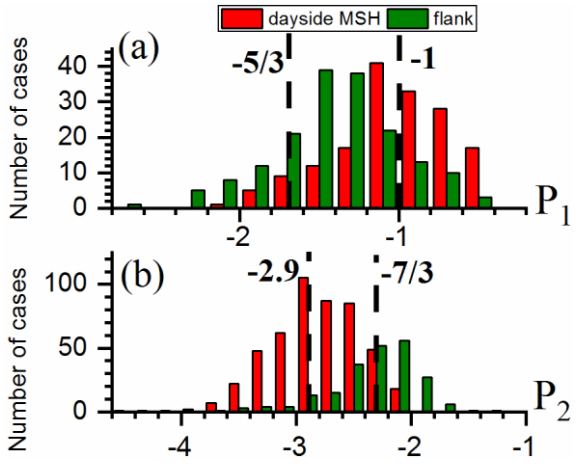

Figure 5. Distribution of spectrum slopes on MHD (*a*) and kinetic (*b*) scales in dayside MSH (red) and on flanks (green)

No statistical studies have previously been conducted on changes in characteristics of fluctuation spectra in MSH at a distance from the subsolar region to –60 R_E. In [Huang et al., 2017; Li et al., 2020], for all the cases considered X_{GSE} exceeded –10 R_E. Huang et al. [2017] have, however, also observed a tendency for the Kolmogorov spectrum shape to recover with distance from the subsolar region of MSH, and the data presented in the work indicates a simultaneous flattening of spectra on kinetic scales, although the authors do not consider this fact as a conclusion. Thus, the statistical material of this work is consistent with the previous results presented in the literature, obtained from data from various spacecraft.

As follows from Figure 1, in the statistical sample under study in dayside MSH and on flanks there are events related to three SW types: undisturbed (including slow and fast quasi-stationary flows), ICME, and CIR. For these SW types, average slopes in both selected MSH regions were analyzed. The results are presented in Figure 6: red symbols are average slopes for dayside MSH; blue ones, for the flank on MHD and kinetic scales. Vertical segments indicate errors in determining the average; numbers of corresponding colors next to

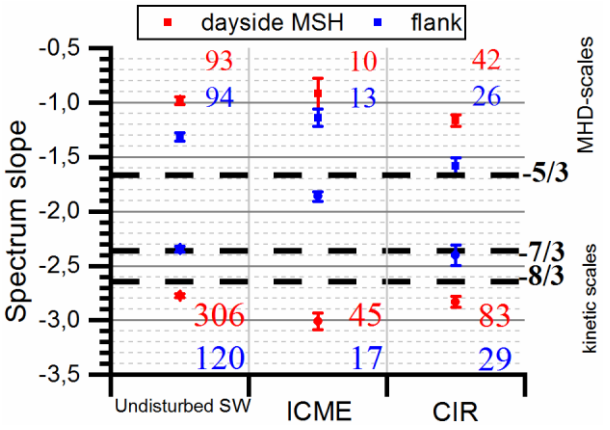

Figure 6. Average spectrum slopes in dayside MSH (red) and on a flank (blue)

the symbols denote the number of events estimated.

Figure 6 shows that the dynamics of characteristics of turbulent fluctuation spectra (see Figure 5) is typical, on average, for all the three SW types considered. There are, however, some special features in each of them.

In dayside MSH on MHD scales, a significant deviation of the spectra from the Kolmogorov scaling is observed for all the SW types. At the same time, the spectra become steeper on the flanks, the slope approaches –5/3. The spectrum type close to the Kolmogorov one on the flanks is, nonetheless, typical only for CIR events.

On kinetic scales, all the SW types are different: spectra on the flanks are flatter than in dayside MSH. In this case, in dayside MSH the slopes for undisturbed SW and CIR are close to –2.8 as predicted in a number of theoretical and model works [Howes et al., 2011] and observed in undisturbed SW [Kiyani et al., 2009; Chen et al., 2010]. For ICMEs, spectra on kinetic scales are steeper with an average value of –3.On MSH flanks for undisturbed SW and for CIRs, the spectrum slope on kinetic scales becomes close to –7/3 as predicted by the theories of kinetic Alfvén wave turbulence [Schekochihin et al., 2009]. For ICMEs, the spectra, however, become even flatter with slopes averaging –1.9, which differs from the slopes predicted earlier in theoretical descriptions.

Thus, the development of a turbulent cascade during plasma propagation from dayside MSH to its flanks is similar for all the SW types of interest, yet for the events related to ICMEs there are more significant differences between turbulence characteristics in dayside MSH and on its flanks.

2.2. Dayside magnetosheath

A number of previous studies have shown that MSH turbulence characteristics depend on the distance to MSH boundaries [Gutynska et al., 2009; Rakhmanova et al., 2018b; Li et al., 2020], the MSH plasma density [Rakhmanova et al., 2022], the SW plasma velocity [Gutynska et al., 2009], and the angle between velocity and magnetic field vectors in MSH [Rakhmanova et al., 2022]. In this paper, we have analyzed the dependences of spectrum slopes on both MHD and kinetic scales on the density, velocity, magnetic field magnitude, plasma parameter β_p

(the ratio of plasma proton thermal pressure to magnetic pressure), the angle between magnetic field and velocity vectors in SW and MS, the angle θ_{BN}, and the distance to MSH boundaries for the three SW types identified above.

For the slope on the MHD scale, we failed to identify any dependence on the above parameters for any of the SW types considered. Figure 7 indicates that the slopes P_2 on kinetic scales in dayside MSH depend on the plasma parameter β_p, the magnetic field magnitude in MSH, the relative distance D to MSH boundaries, the SW bulk speed, and the angle θ_{BN} for three SW types: undisturbed (black), ICME (red), and CIR (blue). Despite the wide variations in parameter values, in some cases the dependences are clearly seen. For clarity, lines indicate the average slope for equal ranges of parameter values; vertical lines denote standard deviations for the selected range of parameter values. All dependences are shown for which the correlation coefficient exceeds 0.5 in modulus for at least one SW type. Correlation coefficients are highlighted in corresponding colors for each SW type. For the other parameters considered, the correlation coefficient did not exceed 0.5.

Values of the parameters considered vary in wide ranges for each of the three SW types. At the same time, for undisturbed SW no connection was found between spectral characteristics and any parameter. From Figure 7 we can deduce that there are features in the formation of a turbulent cascade in MSH for disturbed SW types. There are pronounced dependences of P_2 on β_p for ICME and CIR: the steepest spectra in dayside MSH are observed for low β_p characteristic of regions with a strong magnetic field. In this case, for ICME there is an explicit dependence of P_2 on the magnetic field magnitude, which is most likely to determine the observed dependence on β_p. Yet, for CIRs the dependence on the magnetic field magnitude is weak (the correlation coefficient is –0.28), and there is no dependence on plasma density and temperature.

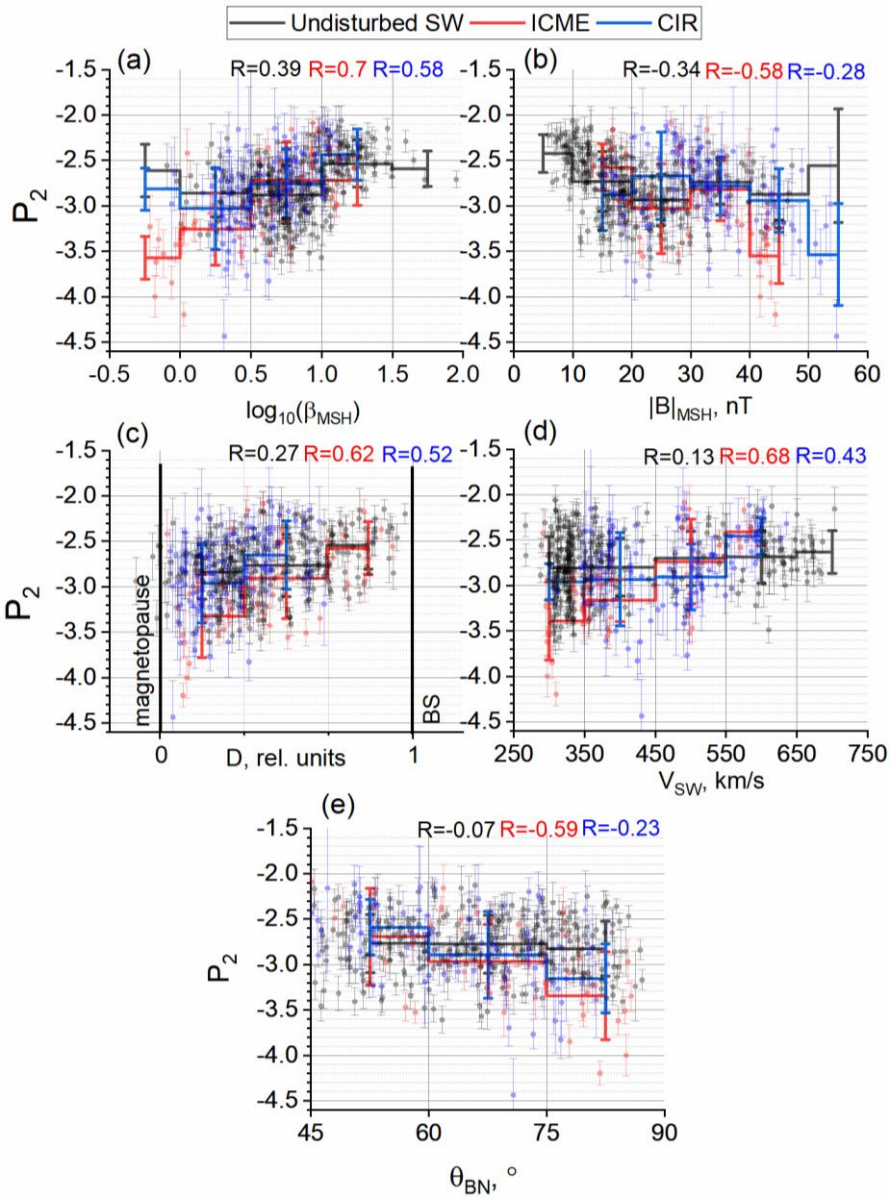

Figure 7. Spectrum slopes P_2 on kinetic scales in dayside MSH as function of plasma parameter β_p (*a*), magnetic field magnitude (*b*), relative distance D to MSH boundaries (*c*), SW plasma velocity (*d*), angle θ_{BN} (*d*)

For both ICME and CIR, a shortening of the spectrum is observed when plasma comes closer to the magnetopause (with a decrease in *D*). For ICME in dayside MSH, the steepest spectra occur when the SW velocity decreases, whereas for velocities higher than 500 km/s the slopes are close to –7/3. A similar tendency is seen for CIRs, but it is less pronounced. Spectra also become steeper with an increase in θ_{BN} for the events related to ICMEs. There is no such dependence for quiet SW and for CIRs.

Note that plasma and magnetic field characteristics can often be interrelated. Obviously, the plasma parameter β_p and the magnetic field magnitude are related by definition. For the ICME statistics considered, higher β_p in MSH is observed at high β_p in SW, which, in turn, occurs at a high plasma velocity during ICME. On average, as follows from [Yermolaev et al., 2015], ejecta-type ICMEs, which are not preceded by sheath and interplanetary shock wave, exhibit lower velocities and lower values of β_p, whereas ICMEs, which are preceded by sheaths, are accompanied by high velocities and β_p. In this paper, ejecta-type ICMEs make up most of the ICME statistics, but there was no selection based on the presence of sheath in front of them. Thus, the SW velocity during ICME and the β_p parameter in the statistics considered are interrelated. Moreover, for the ICME statistics under study a relationship has been found between *D* and β_p: with increasing β_p, *D* increases. This is most likely to be due to the BS dynamics under the impact of ICME: with increasing plasma pressure (i.e., with increasing β_p), the magnetosphere, including the boundary layers, is more compressed and a satellite is closer to BS, located in the same coordinates. Thus, the dependences of P_2 on β_p, magnetic field magnitude, SW velocity, and *D* are interrelated for ICMEs. At the same time, no significant relationship was found between θ_{BN} and each of the above parameters, which suggests that the dependence of P_2 on this parameter is independent. For CIR-type SW, a relationship was found between β_p and *D*, which can also be explained by the above arguments. Thus, for CIR periods we have obtained the dependence of P_2 on two parameters indirectly related to each other.

2.3. Flank

Similarly to dayside MSH, we have analyzed the dependences of spectrum slopes for the three SW types on a number of parameters for the events on the flank.

For the spectrum slope on MHD scales, we failed to identify dependences in the same way as in dayside MSH. Figure 8 illustrates these dependences of P_2 on β_p, MSH magnetic field magnitude, distance to MSH boundaries *D*, and SW velocity. Correlation coefficients for each set of points are highlighted in the corresponding color. Note that the number of events on the flank is significantly smaller than in dayside MSH; therefore, the ranges of plasma and magnetic field parameters are narrower than in Figure 7. Furthermore, due to the smaller number of events, the number of points in Figure 7 allows us to trace dependences without averaging, that is why they are omitted in this case.

According to Figure 8, *a*, there is a relationship between P_2 and the plasma parameter β_p for ICME: the higher is β_p, the steeper are the spectra on the flank, which is opposite to the dependence in dayside MSH. The range of β_p values considered is, however, very narrow, and the statistics includes only 12 points owing to the lack of plasma measurements for some events. At the same time, Figure 8, *b* shows that for ICME there are steeper spectra with an increase in the magnetic field magnitude, which is consistent with the dependence shown in panel *a*. In this case, the number of points is larger than in the β_p dependence since magnetic field measurements are available for all the events. Note that the dependences on magnetic field strength and β_p are opposite to those observed in dayside MSH.

For CIR periods, the dependence of P_2 on β_p is absent on the flank, unlike the clear dependence in dayside MSH. Figure 8, *b* indicates that for these events there is a relationship between the slope on kinetic scales and the magnetic field magnitude: the stronger the magnetic field, the steeper the spectra on the flank, which was not observed in dayside MSH. The obtained dependence on the magnetic field strength for CIR is opposite to the similar dependence for ICME.

According to Figure 8, *b*, during CIR-type SW there is a relationship between P_2 and the distance to MSH boundaries: steeper spectra are observed near the magnetopause. A similar dependence was found in dayside MSH for both CIRs and ICMEs, but on the flank it is observed only for CIRs.

Figure 8, *d* shows that for ICME periods there is a dependence of P_2 on SW velocity, and it is opposite to that observed in dayside MSH: the flattest spectra correspond to lower velocities. For CIRs, the correlation coefficient is –0.61, yet the range of SW velocity values for the events considered is narrow and does not suggest the presence of an unambiguous dependence.

The analysis has revealed that there is no relationship between the magnetic field magnitude, SW velocity and the parameter *D* for all the SW types, i.e. both patterns presented for the CIR type in Figure 8 can be considered independent.

3. DISCUSSION

The statistical analysis of properties of turbulent fluctuation spectra in various MSH regions behind quasi-perpendicular BS for SW of different types allowed us to identify some features of the dynamics of the turbulent cascade behind BS.

On average, spectra with slopes close to –1 on MHD scales are observed in dayside MSH. This is consistent with the results [Huang et al., 2017] obtained from other satellite data. At the same time there is, on average, no difference between slopes on MHD scales for undisturbed SW, ICMEs, and CIRs. Moreover, the spectrum slope does not depend on plasma and magnetic field parameters, θ_{BN}, the distance to MSH boundaries, the mutual direction of magnetic field and velocity vectors. Thus, the properties of the turbulent cascade compressible component in dayside MSH are likely to be determined

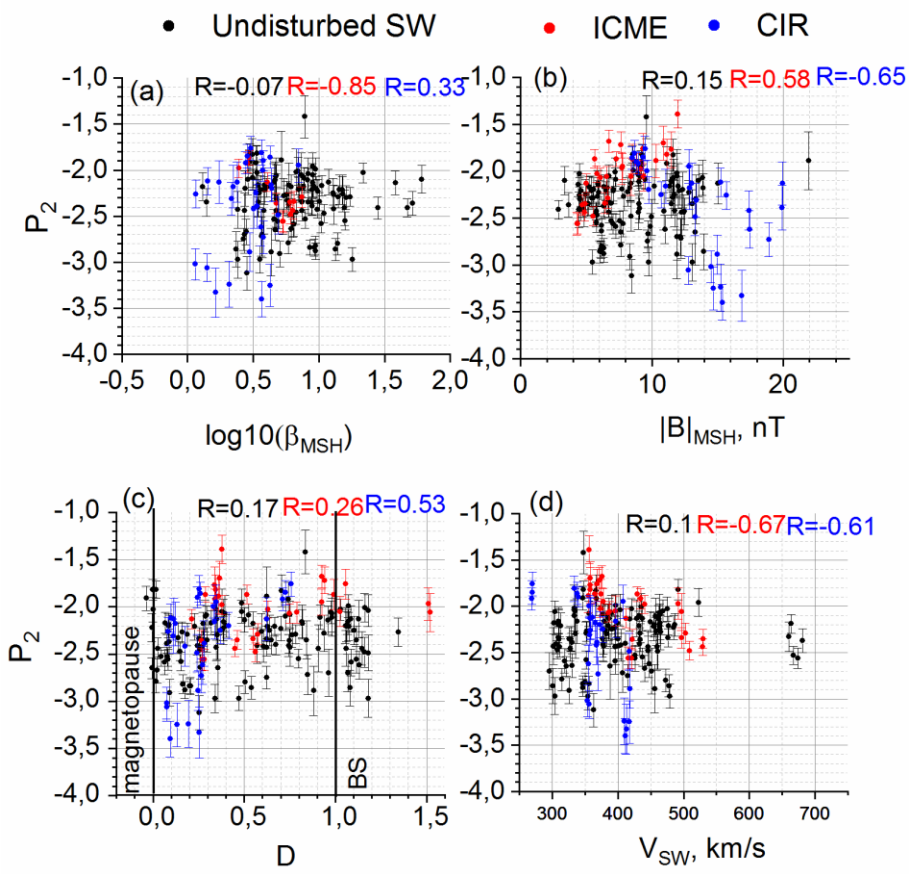

Figure 8. Spectrum slope P_2 on kinetic scales on MSH flanks as function of MSH magnetic field magnitude (*a*), distance to MSH boundaries (*b*), and SW velocity (*c*)

mined by processes in BS, i.e. redistribution of energy in the cascade and violation of the condition of developed turbulence when plasma crosses BS. Hence the conditions observed in dayside MSH differ from predictions of the theories of developed turbulence [Goldreich, Sridar, 1995; Iroshnikov, 1963; Kraichnan et al., 1965] and are more consistent with the assumption that there is no inertial region of cascade and energy dissipation without cascade transmission. Moreover, for all the three SW types considered, this process occurs in the same way. Rakhmanova et al. [2020b] have suggested that Kolmogorov spectra near BS are characteristic only for undisturbed SW. Yet, in this work, the statistics concerned MSH regions located far from the subsolar region and ignored the slope change on MHD scales during plasma propagation along X_{GSE}.

On kinetic scales, there is a difference between the processes occurring in dayside MSH during periods of undisturbed SW and ICME. On average, ICME periods are characterized by steeper spectra with an exponent of –3 than for undisturbed SW and for CIR (with an exponent of –2.8). At the same time, as shown in [Riazantseva et al., 2020], in ICME-type SW itself the spectra on kinetic scales have an average slope of –3, whereas undisturbed SW exhibits a slope of –2.8. The difference between the slopes on kinetic scales in dayside MSH is probably due to the difference between turbulence characteristics in large-scale phenomena in SW. The processes on kinetic scales for ICME periods are controlled by the plasma parameter β_p (namely, the magnetic field strength), the SW velocity, θ_{BN}, and the distance to MSH boundaries: the greatest steeping of spectra occurs at low SW velocities at $\beta_p \square 1$ (high magnetic field strengths), θ_{BN} close to 90°, as well as near the magnetopause.

Disturbed SW (ICME, CIR) features variations in IMF direction, which leads to an increase in the IMF component tangential to BS. Under such conditions, the magnetic field strengthens behind BS, which can cause turbulence to weaken [Barkhatov et al., 2001]. The relationship between turbulence characteristics and the magnetic field strength we have demonstrated in this work can be produced by this effect.

It is worth noting that a characteristic feature of MSH behind quasi-perpendicular BS is a significant temperature anisotropy that generates wave processes, and the process type depends on β_p: at $\beta_p<1$, Alfvén ion cyclotron waves develop; at $\beta_p>5$, mainly mirror mode waves occur which are compression fluctuations [Schwartz, 1996]. This may explain the β_p dependence of the slope on kinetic scales for periods of disturbed SW: at low β_p, the compressible fluctuation component is suppressed and spectra are steeper than those for high β_p, at which there are additional compression fluctuations due to mirror mode waves in the cascade. For quiet SW periods, processes on kinetic scales are mainly determined by other factors.

In addition to β_p and θ_{BN}, there is also a relationship between the spectrum slope in dayside MSH during ICME periods and the SW plasma velocity: the slower is the plasma stream, the steeper is the spectrum on kinetic scales. At the same time, for velocities around 300 km/s, the spectra in MSH have slopes of about –3.5, which is significantly less than described in theories, even taking into account additional factors such as intermittency and Landau damping [Alexandrova et al., 2013], and then usually observed in undisturbed SW [Chen et al., 2013]. For fast SW with speeds higher than 500 km/s, spectrum slopes are close to –7/3 and –8/3 predicted by theories [Schekochihin et al., 2009; Boldyrev, Perez, 2012]. Thus, when ICME arrives with a slow plasma stream, the spectrum shape on kinetic scales is close to that observed in SW and described by the theories of Alfvén wave turbulence, taking into account such factors as, for example, Landau damping [Howes et al., 2011] or the contribution of the compression component of fluctuations [Alexandrova et al., 2007], whereas at high velocities of incoming plasma turbulent fluctuation spectrum properties conform to the theoretical descriptions for the developed turbulence of kinetic Alfvén waves [Schekochihin et al., 2009]. Note that for the CIR-related events slopes on kinetic scales in dayside MSH are also linked to β_p. With equal values of β_p, the spectra on kinetic scales are, however, steeper during ICME periods on average. Besides, only for ICME there is a connection between characteristics of spectra and θ_{BN}, which determines BS properties. These dependences may mean that during ICME periods BS can contribute to the development of turbulence not only on MHD, but also on kinetic scales, contrary to what was previously assumed [Huang et al., 2017].

Unlike undisturbed SW, ICMEs and CIRs are characterized by steeping of spectra on kinetic scales when moving away from BS and approaching the magnetopause. A similar steeping was observed for plasma density and velocity fluctuations in dayside MSH, but it was not detected for magnetic field vector fluctuations [Huang et al., 2017; Li et al., 2020]. Thus, there is a difference in the effect of MSH boundaries on compressible and incompressible components of the cascade.

Note that for ICME the dependences were obtained from the parameters physically related to each other: SW velocity, β_p, and D, which makes it difficult to unambiguously interpret these dependences.

On MSH flanks, there is a steeping of spectra on MHD scales. At the same time, for undisturbed SW the slope of the spectra varies, on average, from –1 to –1.3; for ICMEs, from –0.9 to –1.1; for CIRs, from –1.2 to –1.6. Thus, there is a tendency for the Kolmogorov scaling to recover when plasma moves away from dayside MSH. This recovery is likely due to the nonlinear interactions between fluctuations and the development of a new turbulent cascade when plasma moves away from BS. Nonetheless, this recovery occurs in different ways for different SW types, which is probably determined by the difference in the amount of additional energy supplied to the cascade in BS. The complete recovery of the Kolmogorov scaling at distances around X_{GSE}=–60 R_E occurs only for CIR-type events characterized by a high degree of plasma compression. At the same time, on MHD scales there is no dependence of slopes on any primary plasma and magnetic field parameters, as well as on the distance to MSH boundaries, β_p, and θ_{BN}. Thus, the development of a cascade on MHD scales is determined only by the distance traveled from the MSH subsolar region, and plasma belonging to different SW types requires different time to restore the conditions necessary for the development of a turbulent cascade.

Reconstruction of the Kolmogorov scaling, i.e. the transition to developed turbulence, has been repeatedly observed during plasma propagation to flanks [Huang et al., 2017; Rakhmanova et al., 2022]. Previous studies have not, however, considered at what distance from the subsolar region such a transition occurs. According to the results of our statistical analysis, restoration of the Kolmogorov spectral type begins, on average, at distances X_{GSE} from –10 R_E to –25 R_E. Nonetheless, as mentioned above, this transition probably occurs differently for different SW types and requires a more sophisticated treatment.

On kinetic scales on MSH flanks for undisturbed SW and CIRs, usually there are spectra with a slope of –7/3, often described in theoretical works. For ICMEs, the spectrum slope is, however, significantly lower in modulus and averages –1.9. Thus, during periods of ICME interaction with the magnetosphere, additional compression fluctuations on sub-ion scales develop during plasma propagation from dayside MSH to the flanks.

For the CIR-related events on kinetic scales, the spectrum slope on the flanks, as well as in dayside MSH, is determined by the distance to the magnetopause: the steepest spectra are recorded near the magnetopause. During ICME, such dependence is not observed on the flanks. Thus, the presence of the magnetopause makes a significant contribution to the formation of the compressible component of the turbulent cascade during CIR periods.

Steeping of spectra during CIR periods on the flanks also occurs with an increase in the magnetic field magnitude, not observed in dayside MSH. At the same time, unlike dayside MSH, there is no dependence on β_p. Thus, for CIR events characterized by a high degree of compression, the contribution of different factors to the formation of the cascade changes as plasma moves away from dayside MSH.

For ICME on the flanks, in contrast to dayside MSH, spectra become steeper when the magnetic field magnitude decreases. In statistics there is, however, a rather limited range of values of the magnetic field magnitude for ICME-type events on the flank, so the dependence mentioned for ICME may be an artificial effect associated with sampling.

There is a relationship between processes on kinetic scales on the MSH flank for disturbed SW conditions with the SW plasma velocity: for both ICME and CIR, the spectra become steeper as the SW plasma velocity increases. In dayside MSH, this dependence was inverse for ICME and was weak (0.43 correlation coefficient) for CIR periods. At the same time, for ICME, as the plasma velocity increases both in dayside MSH and on

flanks, spectrum slopes become closer to theoretical predictions. Thus, if a disturbance in SW is accompanied by low plasma velocities, turbulence properties are probably determined by processes in BS, whereas for high SW velocities turbulence characteristics are conditioned by local processes in plasma and "do not feel" the presence of BS.

4. RESULTS

The results we have obtained can be summarized as follows.

1. The absence of the Kolmogorov spectrum in the dayside magnetosheath results only from BS properties and processes in it for all the SW types considered.

2. Further development of the turbulent cascade on MHD scales when plasma moves away from dayside MSH is defined only by the distance traveled, while different SW types require different distances for the development of turbulence and recovery of the Kolmogorov scaling; on average, a return to previous conditions of the developed turbulence becomes observable at distances $-10\ R_E<X_{GSE}<-25\ R_E$.

3. For undisturbed SW, there is no connection between the slopes on kinetic scales and the parameters of surrounding plasma both in dayside MSH and on the flanks; on average, the slope varies from –2.8±0.3 to –2.3±0.3 when plasma moves away from the subsolar region.

4. During ICMEs, spectra steeper than for other SW types with an average slope –3±0.5 are observed on kinetic scales in dayside MSH, and the steepest spectra (with slopes less than –4) exist at $\beta_p \leq 1$ (associated with a high magnetic field value) and with an increase in θ_{BN} up to 90°; at the same time, when plasma propagates to flanks, there are flatter spectra with $P_2 \sim -1.9 \pm 0.2$, which is not typical of other SW types; the flattest spectra take place during periods of slow SW against the background of ICME.

5. During the interaction of CIRs with the magnetosphere in dayside MSH, there are spectra with average slopes –2.8±0.3 on kinetic scales, and they increase in modulus as the spectrum approaches the magnetopause and the plasma parameter β_p decreases; when plasma propagates to flanks, the slope changes on average to –2.4±0.5, meanwhile depending on the distance to the magnetopause.

Thus, for the first time through statistical analysis we have demonstrated a difference in the development of turbulence in boundary layers of Earth's magnetosphere for large-scale phenomena of the interplanetary medium characterized by different geoeffectiveness, which may suggests that the magnetosheath turbulence contributes to the geoeffectiveness of the events in the solar wind.

The work was financially supported by the Russian Science Foundation (Grant No. 22-72-00105) [https://rscf.ru/project/22-72-00105/].

REFERENCES

Alexandrova O., Mangeney A., Maksimovic M., Cornilleau-Wehrlin N., Bosqued J.-M., André M. Alfvén vortex filaments observed in magnetosheath downstream of a quasi-perpendicular bow shock. *J. Geophys. Res.* 2006, vol. 111, A12208. DOI: 10.1029/2006JA011934.

Alexandrova O., Carbone V., Veltri P., Sorriso-Valvo L. Solar wind cluster observations: turbulent spectrum and role of Hall effect. *Planetary Space Sci*. 2007, vol. 55, pp. 2224–2227. DOI: 10.1016/j.pss.2007.05.022.

Alexandrova O., Lacombe C., Mangeney A. Spectra and anisotropy of magnetic fluctuations in the Earth's magnetosheath: cluster observations. *Ann. Geophys*. 2008, vol. 26, pp. 3585–3596. DOI: 10.5194/angeo-26-3585-2008.

Alexandrova O., Saur J., Lacombe C., Mangeney A. Universality of solar-wind turbulent spectrum from MHD to electron scales. *Phys. Rev. Lett*. 2009, vol. 103, no. 16, 165003. DOI: 10.1103/PhysRevLett.103.165003.

Alexandrova O., Chen C.H.K., Sorriso-Valvo L., Horbury T.S., Bale S.D. Solar wind turbulence and the role of ion instabilities. *Space Sci. Rev*. 2013, vol. 178, pp. 101–139. DOI: 10.1007/s11214-013-0004-8.

Angelopoulos V. The THEMIS Mission. *Space Sci.Rev*. 2008. Vol. 141. P. 5–34. DOI: 10.1007/s11214-008-9336-1.

Auster H.U., Glassmeier K.H., Magnes W., Aydogar O., Baumjohann W., Constantinescu D., Fische, D., Fornacon, K.H., Georgescu E., Harvey P., et al. The THEMIS fluxgate magnetometer. *Space Sci. Rev*. 2008, vol. 141,pp. 235–264. DOI: 10.1007/s11214-008-9365-9.

Bandyopadhyay R., Matthaeus W.H., Parashar T.N., Yang Y., Chasapism A., Giles B., Gershman D., Pollock C., Russell C., Strangeway R., et al. Statistics of kinetic dissipation in the Earth's magnetosheath: MMS observations. *Phys. Rev. Lett.* 2020, vol. 124, 255101. DOI: 10.1103/PhysRevLett.124.255101.

Barkhatov N.A., Belliustin N.S., Bougeret J.-L., Sakharov S.Yu., Tokarev Yu.V. Influence of the solar wind magnetic field on the Earth's magnetosheath turbulence behind the bow shock. *Radiophysics and Quantum Electronics*. 2001, vol. 44, pp. 993–1002. DOI: 10.1023/A:1014828310176.

Barkhatov N.A., Vorobjev V.G., Revunov S.E., Barkhatova O.M., Yagodkina O.I. Substorm Activity and Orientation of the Front of a Shock Wave of an Interplanetary Magnetic Cloud. *Geomagnetism and Aeronomy*. 2019, vol. 59, no. 4, pp. 398–406. DOI: 10.1134/S0016793219040042.

Barkhatova O.M., Vorobjev V.G., Barkhatov N.A., Revunov S.E. ULF Disturbances Caused by the Turbulent Sheath of Interplanetary Magnetic Clouds. *Bulletin of the Russian Academy of Sciences: Physics*. 2021, vol. 85, no. 3, pp. 238–241. DOI: 10.3103/S1062873821030060.

Boldyrev S., Perez J.C. Spectrum of kinetic Alfven turbulence. *Astrophys. J. Lett.* 2012, vol. 758, no. 2, p. 5. DOI: 10.1088/2041-844 8205/758/2/L44.

Borovsky J.E. The velocity and magnetic field fluctuations of the solar wind at 1 AU: Statistical analysis of Fourier spectra and correlations with plasma properties. *J. Geophys. Res.* 2012, vol. 117, A05104. DOI: 10.1029/2011JA017499.

Bruno R., Carbone V. The solar wind as a turbulence laboratory *Living Reviews in Solar Physics.* 2013, vol. 10, p. 7. DOI: 10.12942/ lrsp-2013-2.

Chen C.H.K., Boldyrev S. Nature of kinetic scale turbulence in the Earth's magnetosheath. *Astrophys. J.* 2017, vol. 842, 122. DOI: 10.3847/1538-4357/aa74e0.

Chen C.H.K., Horbury T.S., Schekochihin A.A., Wicks R.T., Alexandrova O. Mitchell, J. Anisotropy of solar wind turbulence between ion and electron scales. *Phys. Rev. Lett.* 2010, vol. 104, 255002. DOI: 10.1103/PhysRevLett.104.255002.

Chen C.H.K., Boldyrev S., Xia Q., Perez J.C. Nature of Subproton Scale Turbulence in the Solar Wind. *Phys.Rev. Lett.* 2013, vol. 110, no. 22, 225002. DOI: 10.1103/PhysRevLett.110.225002.

Chen C.H., Leung L., Boldyrev S., Maruca B.A., Bale S.D. Ion-scale spectral break of solar wind turbulence at high and low

beta. *Geophys. Res. Lett.* 2014, vol. 41, pp. 8081–8088. DOI: 10.1002/2014 GL062009.

Goldreich P., Sridhar S. Toward a theory of interstellar turbulence. II. Strong Alfvénic turbulence. *Astrophys. J.* 1995, vol. 438, pp. 763–775. DOI: 10.1086/175121.

Greenstadt E.W. Binary index for assessing local bow shock obliquity. *J. Geophys. Res.* 1972, vol. 77, pp. 5467–5479. DOI: 10.1029/JA077i028p05467.

Gutynska O., Šafránková J., Němeček Z. Correlation properties of magnetosheath magnetic field fluctuations. *J. Geophys. Res.* 2009, vol. 114, A08207. DOI: 10.1029/2009JA014173.

Howes G.G., TenBarge J.M., Dorland W., Quataert E., Schekochihin A.A, Numata R., Tatsuno T. Gyrokinetic simulations of solar wind turbulence from ion to electron scales. *Phys. Rev. Lett.* 2011, vol. 107, no. 3, 035004. DOI: 10.1103/PhysRevLett.107.035004.

Huang S.Y., Sahraoui F., Deng X.H., He J.S., Yuan Z.G., Zhou M., Pang Y., Fu H.S. Kinetic turbulence in the terrestrial magnetosheath: Cluster observations. *Astrophys. J.* 2014, vol. 789, L28. DOI: 10.1088/2041-8205/789/2/L28.

Huang S.Y., Hadid L.Z., Sahraoui F., Yuan Z.G., Deng X.H. On the existence of the Kolmogorov inertial range in the terrestrial magnetosheath turbulence. *Astrophys. J. Lett.* 2017, vol. 836, no. 1, L10. DOI: 10.3847/2041-8213/836/1/L10.

Iroshnikov P.S. Turbulence of a Conducting Fluid in a Strong Magnetic Field. *Soviet Astronomy*. 1964, vol. 7, p. 566.

Kiyani K.H., Chapman S.C., Khotyaintsev Y.V., Dunlop M.W., Sahraoui F. Global scale-invariant dissipation in collisionless plasma turbulence. *Phys. Rev. Lett.* 2009, vol. 103, no. 7, 075006. DOI: 10.1103/PhysRevLett.103.075006.

Kiyani K.H., Osman K.T., Chapman S.C. Dissipation and heating in solar wind turbulence: from the macro to the micro and back again. *Philosophical Trans. of the Royal Society of London. Ser. A.*, 2015, 373:20140155. DOI: 10.1098/rsta.2014.0155.

Klein K.G., Howes G.G., Tenbarge J.M. The violation of the taylor hypothesis in measurements of solar wind turbulence. *Astrophys. J. Lett.* 2014, vol. 790, 20. DOI: 10.1088/2041-8205/790/2/L20.

Kraichnan R.H. Inertial-Range Spectrum of Hydromagnetic Turbulence. *Phys. Fluids.* 1965, vol. 8, pp. 1385–1387. DOI: 10.1063/1.1761412.

Lacombe C., Belmont G. Waves in the Earth's magnetosheath: observations and interpretations. *Adv. Space Res.* 1995, vol. pp. 329–340. DOI: 10.1016/0273-1177(94)00113-F.

Lacombe C., Alexandrova O., Matteini L., Santolík O., Cornilleau-Wehrlin N., Mangeney A., de Conchy Y., Maksimovic M. Whistler Mode Waves and the Electron Heat Flux in the Solar Wind: Cluster Observations. *Astrophys. J.* 2014, vol. 796, no. 1, p. 5. DOI: 10.1088/0004-637X/796/1/5.

Lepping R.P., Acũna M.H., Burlaga L.F., Farrell W.M., Slavin J.A., Schatten K.H., Mariani F., Ness N.F., Neubauer F.M., Whang Y.C., et al. The WIND magnetic field investigation. *Space Sci Rev.* 1995, vol. 71, pp. 207–229. DOI: 10.1007/BF00751330.

Li H., Jiang W., Wang C., Verscharen D., Zeng C. Russell C.T., Giles B., Burch J.L. Evolution of the Earth's magnetosheath turbulence: a statistical study based on MMS observations. *Astrophys. J.*, 2020, vol. 898, L43. DOI: 10.3847/ 2041-8213/aba531.

Macek W.M., Krasinska A., Silveira M.V.D., Sibeck D.G., Wawrzaszek A., Burch J.L., Russell C.T. Magnetospheric multiscale observations of turbulence in the magnetosheath on kinetic scales. *Astrophys. J.* 2018, vol. 864, L29. DOI: 10.3847/2041-8213/aad9a8.

Ogilvie K.W., Chornay D.J., Fritzenreiter R.J., Hunsaker F., Keller J., Lobell J., Miller G., Scudder J.D., Sittler Jr. E.C., Torbert R.B., et al. SWE, a comprehensive plasma instrument for the WIND spacecraft. *Space Sci Rev.* 1995, V. 71, P. 55–77. DOI: 10.1007/BF00751326.

Rakhmanova L., Riazantseva M., Zastenker G. Plasma fluctuations at the flanks of the Earth's magnetosheath at ion kinetic scales. *Ann. Geophys.* 2016, vol. 34, pp. 1011–1018. DOI: 10.5194/angeo-34-1011-2016.

Rakhmanova L., Riazantseva M., Zastenker G., Verigin M. Kinetic scale ion flux fluctuations behind the quasi-parallel and quasi-perpendicular bow shock. *J. Geophys. Res.: Space Phys.* 2018a, vol. 123, pp. 5300–5314. DOI: 10.1029/2018JA025179.

Rakhmanova L.S., Riazantseva M.O., Zastenker G.N., Verigin M.I. Effect of the magnetopause and bow shock on characteristics of plasma turbulence in the Earth's magnetosheath, *Geomagnetism and Aeronomy*. 2018b, vol. 58, pp. 718–727. DOI: 10.1134/S0016793218060129.

Rakhmanova L.S., Riazantseva M.O., Zastenker G.N., Yermolaev Y.I., Lodkina I.G., Chesalin L.S. Turbulent cascade in the magnetosheath affected by the solar wind's plasma turbulence. *Cosmic Res.* 2019, vol. 57, pp. 443–450. DOI: 10.1134/S0010952519060066.

Rakhmanova L.S., Riazantseva M.O., Zastenker G.N., Yermolaev Y.I., Lodkina I.G. Dependence of the properties of a turbulent cascade behind the bow shock on the dynamics of the solar wind parameters. *Cosmic Res.* 2020a, vol. 58, no. 6, pp. 478–486. DOI: 10.1134/S0010952520060088.

Rakhmanova L., Riazantseva M., Zastenker G., Yermolaev Y., Lodkina I. Dynamics of plasma turbulence at Earth's bow shock and through the magnetosheath. *Astrophys. J.* 2020b, vol. 901, 30. DOI: 10.3847/ 1538-4357/abae00.

Rakhmanova L., Riazantseva M., Zastenker G. Plasma and magnetic field turbulence in the Earth's magnetosheath at ion scales. *Front. Astron. Space Sci.* 2021, vol. 7, 616635. DOI: 10.3389/fspas.2020.616635.

Rakhmanova L., Riazantseva M., Zastenker G., Yermolaev Y. Large-scale solar wind phenomena affecting the turbulent cascade evolution behind the quasi-perpendicular bow shock. *Universe*. 2022, vol. 8, no. 12, 611. DOI: 10.3390/universe8120611.

Rakhmanova L., Riazantseva M., Zastenker G., Yermolaev Y. Role of the variable solar wind in the dynamics of small-scale magnetosheath structures. *Front. Astron. Space Sci.* 2023, 10:1121230. DOI: 10.3389/fspas.2023.1121230.

Riazantseva M.O., Budaev V.P., Zelenyi L.M., Zastenker G.N., Pavlos G.P., Safrankova J., Nemecek Z., Prech L., Nemec F. Dynamic properties of small-scale solar wind plasma fluctuations. *Philosophical Trans. of the Royal Society of London. Ser. A.* 2015, vol. 373, 20140146. DOI: 10.1098/rsta.2014.0146.

Riazantseva M.O., Rakhmanova L.S., Zastenker G.N., Yermolaev Yu.I., Lodkina I.G., Chesalin L.S. Small-Scale Plasma Fluctuations in Fast and Slow Solar Wind Streams. *Cosmic Res.* 2020, vol. 57, no. 6, pp. 434–442.

Roberts O.W., Narita Y., Nakamura R., Vörös Z., Gershman D. Anisotropy of the spectral index in ion scale compressible turbulence: MMS observations in the magnetosheath. *Front. Phys.* 2019, vol. 7, 184. DOI: 10.3389/fphy.2019.00184.

Safránková J., Němeček Z., Němec F., Přech L., Pitňa A., Chen C.H.K., Zastenker G.N. Solar wind density spectra around the ion spectral break. *Astrophys. J.* 2015, vol. 803, 107. DOI: 10.1088/0004-637X/803/2/107.

Sahraoui F., Belmont G., Rezeau L., Cornilleau-Wehrlin N., Pinçon J.L., Balogh A. Anisotropic turbulent spectra in the terrestrial magnetosheath as seen by the cluster spacecraft. *Phys. Rev. Lett.* 2006, vol. 96, 075002. DOI: 10.1103/PhysRevLett.96.075002.

Sahraoui F., Hadid L., Huang S. Magnetohydrodynamic and kinetic scale turbulence in the near-Earth space plasmas: a

(short) biased review. *Rev. Modern Physics*. 2020, vol. 4, 4. DOI: 10.1007/s41614-020-0040-2.

Schekochihin A.A., Cowley S.C., Dorland W., Hammett G.W., Howes G.G., Quataert E., Tatsuno T. Astrophysical gyrokinetics: kinetic and fluid turbulent cascades in magnetized weakly collisional plasmas. *Astrophys. J. Suppl.*, 2009, vol. 182, pp. 310–377. DOI: 10.1088/0067-0049/182/1/310.

Schwartz S.J., Burgess D., Moses J.J. Low-frequency waves in the Earth's magnetosheath: present status. *Ann. Geophys*. 1996, vol. 14, pp. 1134–1150. DOI: 10.1007/s00585-996-1134-z

Shevyrev N., Zastenker G.N., Nozdrachev M.N., Němeček Z., Šafránková J., Richardson J.D. High and low frequency large amplitude variations of plasma and magnetic field in the magnetosheath: radial profile and some features. *Adv. Space Res*. 2003, vol. 31, no. 5, pp. 1389–1394. DOI: 10.1016/S0273-1177(03)00008-5.

Shue J.-H., Song P., Russell C.T., Steinberg J.T., Chao J.K., Zastenker G., Vaisberg O.L. Kokubun S., Singer H.J., Detman T.R., Kawano H. Magnetopause location under extreme solar wind conditions. *J. Geophys. Res.* 1998, vol. 103, no. A8, pp. 17691–17700. DOI: 10.1029/98JA01103.

Spreiter J.R., Summers A.L., Alksne A.Y. Hydromagnetic flow around the magnetosphere. *Planet. Space Sci.* 1966, vol. 14, pp. 223–253.

Stawarz J.E., Eastwood J.P., Phan T.D., Gingell I.L., Shay M.A., Burch J.L., Ergun R.E., Giles B.L., Gershman D.J., Le Contel O., et al. Properties of the turbulence associated with electron-only magnetic reconnection in Earth's magnetosheath. *Astrophys. J.* 2019, vol. 877, L37. DOI: 10.3847/2041-8213/ab21c8.

Taylor G.I. The spectrum of turbulence. *Proc. R. Soc. A Math. Phys. Eng. Sci.* 1938, vol. 164, pp. 476–490. DOI: 10.1098/rspa.1938.0032.

Verigin M.I., Kotova G.A., Slavin J., Szabo A., Kessel M., Safrankova J., Nemecek Z., Gombosi T.I., Kabin K., Shugaev F., Kalinchenko A. Analysis of the 3-D shape of the terrestrial bow shock by Interball/Magion 4 observations. *Adv. Space Res*. 2001, vol. 28, no 6, pp. 857–862. DOI: 10.1016/S0273-1177(01)00502-6.

Vörös Z., Yordanova E., Khotyaintsev Y.V., Varsan, A., Narita Y. Energy conversion at kinetic scales in the turbulent magnetosheath. *Frontiers in Astronomy and Space Sciences. Sci*.. 2019, vol. 6, 60. DOI: 10.3389/fspas.2019.00060.

Yermolaev Yu.I., Nikolaeva N.S., Lodkina I.G., Yermolaev M.Yu. Catalog of large-scale solar wind phenomena during 1976–2000. *Cosmic Res.* 2009, vol. 47, no. 2, pp. 81–94.

Yermolaev Y.I., Lodkina I.G., Nikolaeva N.S., Yermolaev M.Y. Dynamics of large-scale solar-wind streams obtained by the double superposed epoch analysis. *J. Geophys. Res.: Space Phys*. 2015, vol. 120, pp. 7094–7106. DOI: 10.1002/ 2015JA021274.

Yordanova E., Vaivads A., André M., Buchert S.C., Vörös Z. Magnetosheath plasma turbulence and its spatiotemporal evolution as observed by the cluster spacecraft. *Phys. Rev. Lett.* 2008, vol. 100, 205003. DOI: 10.1103/PhysRevLett.100.205003.

Yordanova E., Vörös Z., Raptis S., Karlsson T. Current sheet statistics in the magnetosheath. *Front. Astron. Sp. Sci*. 2020, vol. 7, 2. DOI: 10.3389/fspas.2020.00002.

URL: https://themis.ssl.berkeley.edu/orbits (accessed November 23, 2023).

URL: http://www.iki.rssi.ru/pub/omni (accessed November 23, 2023).

URL: https://rscf.ru/project/22-72-00105/ (accessed November 23, 2023).

Original Russian version: Rakhmanova L.S., Khokhlachev A.A., Riazantseva M.O., Yermolaev Y.I., Zastenker G.N., published in Solnechno-zemnaya fizika. 2024. Vol. 10. Iss. 2. P. 15–28. DOI: 10.12737/szf-102202402.

How to cite this article

Rakhmanova L.S., Khokhlachev A.A., Riazantseva M.O., Yermolaev Y.I., Zastenker G.N. Turbulence development behind the bow shock during disturbed and undisturbed solar wind. *Solar-Terrestrial Physics*. 2024. Vol. 10. Iss. 2. P. 13–25. DOI: 10.12737/stp-102202402.